Clays and Clay Minerals (2024), **72**, e32, 1–9
doi:10.1017/cmn.2024.26

Original Paper

Ionic dissolution and structural evolution of chrysotile and lizardite at the mineral–water interface: reactions in sulfuric acid solution

Dingran Zhao[1,2], Hongjuan Sun[1,2], Tongjiang Peng[2] and Li Zeng[1,2]

[1]Key Laboratory of Ministry of Education for Solid Waste Treatment and Resource Recycle, Southwest University of Science and Technology, Mianyang, Sichuan 621010, China and [2]Institute of Mineral Materials and Applications, Southwest University of Science and Technology, Mianyang, Sichuan 621010, China

Abstract

Serpentine is widely distributed in the regolith and occurs in different types (chrysotile, lizardite, antigorite). The physical and chemical processes such as composition dissolution and structure evolution of serpentine occur constantly under the action of aqueous solutions. Based on the similarities and differences of polysomic structures and properties of chrysotile (tubular shapes) and lizardite (flat structural layers), the mineral–water interfacial reaction of these two minerals was carried out in a sulfuric acid solution with a concentration of 1 mol L^{-1}. The mineral samples were characterized by powder X-ray diffraction, Fourier-transform infrared spectroscopy, scanning and transmission electron microscopy, Brunauer–Emmett–Teller surface area analysis, magic angle spinning nuclear magnetic resonance, and inductively coupled plasma mass spectrometry. The Si, Mg, and Fe dissolution concentrations, dissolution rates, and dissolution rules and structural changes of chrysotile and lizardite were studied and compared. The results show that H^+ is more aggressive toward lizardite in sulfuric acid solution. The dissolution rate of Si, Mg, and Fe was faster, the dissolution concentration was greater, and structural changes occurred preferentially in lizardite. Specifically, Mg dissolved first in the octahedral sheets, and Si and Fe dissolved later in the tetrahedral sheets. After the water interfacial reaction with the sulfuric acid solution, the ion dissolution rates of both chrysotile and lizardite were Mg > Fe > Si. In summary, this work investigates the mineral–water interfacial reaction of chrysotile and lizardite in sulfuric acid media from different crystal structures and demonstrates that the crystal structure has a significant effect on the acid reactivity of lizardite minerals. Furthermore, the crystal chemistry patterns for the structural dissociation of different two-dimensional structural units were studied. This work provides a mineralogical basis for the study of the mechanisms of ion migration and crystal-structure evolution of serpentine under acidic media.

Keywords: chrysotile; ionic dissolution; lizardite; mineral–water interfacial reactions; structural changes

(Received: 04 January 2024; revised: 14 May 2024; accepted: 08 July 2024)

Introduction

Mineral–water interfacial reactions are involved in many geochemical processes, such as crystallization, erosion, metamorphism, weathering, and the formation of clay minerals (Abad et al., 2022; Li et al., 2022; Locati et al., 2022). During these geological processes, the chemical components of minerals are dissolved, transported and enriched by the aqueous medium. Microbial and animal reproduction and growth, and industrial development can make water bodies slightly acidic (Palmieri et al., 2019; Ren et al., 2023), increasing the rate and complexity of reactions at the mineral–water interface. Serpentine is a common mineral that undergoes constant physical or chemical processes of refinement, component dissolution, structural evolution and reorganization when interacting with slightly acidic aqueous solutions, and is important for maintaining the function of the Earth's ecosystem (Hao et al., 2019).

Corresponding author: Hongjuan Sun; Email: sunhongjuan@swust.edu.cn
Cite this article: Zhao D., Sun H., Peng T., & Zeng L. (2024). Ionic dissolution and structural evolution of chrysotile and lizardite at the mineral–water interface: reactions in sulfuric acid solution. *Clays and Clay Minerals* **72**, e32, 1–9.
https://doi.org/10.1017/cmn.2024.26

In recent years, product leaching, the acid-etching mechanism and acid-etching dissolution kinetics of serpentine in acidic conditions have been studied extensively (Daval et al., 2013; Thomassin et al., 1977). Researchers have found that during the interaction of serpentine with inorganic acid solutions, the different octahedral and tetrahedral sheet components show different dissolution characteristics. The ordered lamellar structure of serpentine disappears gradually, while the specific surface area, maximum adsorption capacity and pore volume increase with the increase in the dissolution rate. In addition, the hydroxyl group and Mg can be removed sequentially from the octahedral sheets, and the residual Si-O tetrahedral sheets can be reconstituted. Furthermore, Mg can be removed by immersing chrysotile in inorganic acid solutions. Fourier-transform infrared (FTIR) spectroscopy and transmission electron microscopy (TEM) studies show that chrysotile formed fibrous SiO_2 after an inorganic acid attack, maintaining the fibrous morphology of the original mineral (Wang et al., 2006). The zeta potential tests and dissolution tests on serpentine revealed that the isoelectric point (11.9) was greater than other Mg-silicate minerals, and that the hydroxyl groups on the Mg-O octahedral layer in serpentine

were more soluble than Mg^{2+} (Bo et al., 2013). Most past mineral acid-leaching studies have focused on only one serpentine type, such as lizardite acid leaching for Mg extraction (Sanna et al., 2013; Liu et al., 2022) and *in situ* carbon capture and storage (Krevor and Lackner, 2011; Lacinska et al., 2016; Farhang et al., 2019). In contrast, chrysotile has been used mainly for acid leaching to detoxify and prepare (Turci et al., 2007; Turci et al., 2008; Lavkulich et al., 2014; Valouma et al., 2016) novel nanomaterials (Wang et al., 2006; Liu et al., 2007; Habaue et al., 2008; Silva et al., 2011). Overall, more studies have been conducted on the acid leaching rates and product properties of different components of serpentine in acidic water systems. However, few studies have been carried out on the process of serpentine – water interfacial reactions. Few studies were conducted on the dissolution rates of different components, comparative studies on the dissolution of components and structural evolution of different types of serpentines, and dissolution ratios and dissolution rates of Si, Mg, and Fe.

Serpentine minerals are trioctahedral layered silicates with a 1:1 structural layer and the crystal formula $Mg_3[Si_2O_5](OH)_4$. They may be important contributors to the partial melting process in the mantle wedges, and key players in continental rifting and oceanic spreading events (Hirth and Guillot, 2013). They might hold some answers to the origin of life as the serpentinization process may produce abundant H_2-rich fluids to power anaerobic microorganism communities (Corliss et al., 1981; Sleep et al., 2004; Evans, 2010; Huang et al., 2023). Serpentine minerals also can bring large quantities of water from the surface to the deep interior of the Earth via slab-subduction, and affect the global water cycle at a time scale of about 10 million years (Hermann, 2022). In the crystal structure, the structural layers are formed by hydrogen bonding silicon-oxygen tetrahedral sheets (T) and hydroxide magnesite octahedral sheets (O). Due to the smaller size of the tetrahedral sheet compared with the octahedral sheet along the structural layer, deformation of the tetrahedral and octahedral sheets occurs, enhancing the bonding forces. This can be achieved by replacing Mg^{2+} with cations of smaller radii (e.g. Al^{3+}, Fe^{3+}, etc.) in the octahedral sheet and replacing Si^{4+} with cations of larger radii (e.g. Al^{3+}, Fe^{3+}, etc.) in the tetrahedral sheet, with the appropriate adjustment of the atomic positions. Alternatively, coordination is achieved through the curling of the structural layers and the reorienting of the active oxygen of the silica-oxygen tetrahedral sheets to produce periodic inversions and bending of the structural layers (Bailey, 1969; Mével, 2003; Liu et al., 2023). This results in the formation of lizardite with flat structural layers (Fig. 1a), chrysotile with tubular shapes (Fig. 1b), and wavy antigorite (Fig. 1c).

The present study aimed to analyze and compare ion dissolution and structural changes occuring during the mineral–water interfacial reaction between chrysotile and lizardite. The results serve as a theoretical basis for weathering and alteration of chrysotile and lizardite.

Materials and methods

Raw materials

Chrysotile samples were taken from the Mangya asbestos mine in Qinghai Province, China. The samples were crushed and hand-picked under a binocular microscope to remove magnetite and other clearly identifiable impurities. The purified samples were examined using light microscopy (LM), X-ray diffraction (XRD) analysis and scanning electron microscopy (SEM) to ensure that the samples were >98% pure. The fibrous samples were white, filamentous, and pliable, with lengths ranging from a few millimeters to several centimeters. The lizardite samples were obtained from the Beiwagou Cuiyu jade mine, Xiuyan County, Liaoning Province, China. The samples were crushed, ground, passed through a 200-mesh sieve and rinsed ultrasonically three times with anhydrous ethanol to remove impurities.

Material characterization

Specific surface and porosity analyzer Brunauer - Emmett - Teller (BET)

The specific surface area of the samples was analyzed and tested using a McASAP 2460 instrument (Norcross, GA, USA). X-ray diffraction (XRD) was used to determine the mineralogical changes in the samples before and after the mineral–water interfacial reaction. XRD data were obtained using a D/max-IIIA diffractometer manufactured by Rigaku (Tokyo, Japan). A copper target with a sum-tube voltage of 40 kV and a sum-tube current of 40 mA accompanied in this study by a slit system DS1/2(°). The powdered samples were analyzed between 3 and 80°2θ, with a step size of 0.02°2θ, and the scan rate of 2 s per step. FTIR was used to determine the changes in crystal chemistry before and after the mineral–water interfacial reaction. The FTIR spectra were measured using a Frontier spectrometer from Perkin Elmer Instruments (Suzhou, China), using the KBr pressed pellet technique. For this, a 0.9 mg aliquot of a dried subsample was mixed with 80.0 mg of oven-dried, spectroscopic-grade KBr salt (refractive index 1.559, particle diameter 5–20 μm), and the mixture was then ground for 1 min. The mixture was pressed in a die with 10 t of pressure applied for 1 min to form a disc or pellet. The spectra were measured at room temperature, in a test range of 4000–400 cm^{-1} and 64 scans. The cation content (Si, Mg, Fe) in solution was measured by an inductively coupled plasma emission spectrometer (ThermoiCAP 6500, Waltham, MA, USA). The ^{29}Si magic angle spinning nuclear magnetic resonance (MAS NMR) experiments were performed on an Agilent 600M spectrometer (Santa Clara, CA, USA) with a ^{29}Si single pulse magic angle spin resonance frequency of 199.13 MHz, a magic angle spin speed of 8 kHz, and a π/2 pulse width of 4 μs. The chemical shifts of ^{29}Si were calibrated with reference to the TMS solution. Scanning electron microscopy (SEM) was conducted to study the micro-morphology of the samples, using a ZEISS Supra 55 Sapphire (Jena, Thuringen, Germany) field

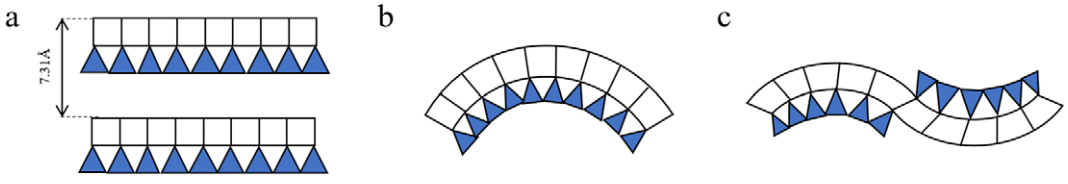

Figure 1. Schematic representation of serpentine minerals crystal structure, including (a) flat layer lizardite, (b) tubular chrysotile, and (c) modulated antigorite.

https://doi.org/10.1017/cmn.2024.26 Published online by Cambridge University Press

Table 1. Chemical composition of chrysotile and lizardite mineral samples (wt.%)

Sample	SiO_2	MgO	Fe_2O_3	K_2O	BaO	NiO	Al_2O_3	SO_3	TiO_2	CaO	MnO	Cr_2O_3	Loss	All
XS	41.69	40.68	1.72	0.50	0.42	0.34	0.33	0.18	0.10	0.02	0.02	0.01	13.98	100.00
LS	38.93	37.46	6.88	0.59	0.30	0.26	1.08	0.17	0.10	0.10	0.09	0.36	13.67	100.00

Table 2. Elemental analysis of the liquid phase at the water interface of chrysotile and lizardite (mg)

	Si		Mg		Fe		Mg/Si	
Time	XSS	LSS	XSS	LSS	XSS	LSS	XSS	LSS
1 h	0.77	1.38	6.47	13.20	0.20	1.45	8.39	9.57
2 h	0.89	1.93	9.19	18.98	0.27	2.01	10.33	9.83
4 h	0.97	2.08	10.13	22.96	0.37	2.36	10.43	11.05
12 h	2.29	3.87	23.44	57.41	0.77	5.33	10.26	14.83
24 h	3.62	4.68	35.31	78.08	1.08	7.22	9.76	16.68
72 h	5.14	5.20	63.65	118.68	2.39	11.59	12.39	19.14
120 h	4.68	6.06	80.29	135.38	3.22	13.53	17.17	22.33
168 h	4.48	5.72	94.03	166.74	3.87	14.63	20.98	29.15
216 h	4.28	5.49	103.58	171.92	4.37	15.32	24.19	31.34

XSS and LSS are defined in the experimental procedure section.

emission scanning electron microscope. The samples were spread onto conductive carbon tape, and the surface was carbon-sprayed before being placed in the sample chamber, vacuumed and observed at an accelerating voltage of 30 kV. Transmission electron microscopy (TEM) was carried out on an American-FEI-Talos F200S (Hillsboro, OR, USA) microscope, accelerated at 200 kV. The chrysotile and lizardite samples were sonicated and dispersed in ethanol for 10 min, then the sample suspension drops were placed on a 200-mesh carbon-coated Cu grid for at least 10 min before being transferred to the microscope.

The average rate of dissolution of each ion in the mineral can be calculated from the following equation:

$$r_i(t) = \frac{C_i \times m_1}{t \times m_0 \times SSA \times \eta_i}, \quad (1)$$

where C_i is the concentration of solute i (Si, Mg, Fe; mmol kg^{-1}) in the sample recovered at time t; m_1 is the mass of the sample solution before sampling (in kg); t is the sample reaction time (s); m_0 is the initial mass of the mineral (g); SSA (m^2 g^{-1}) is the specific surface area of the mineral; and η_i is the stoichiometric coefficient of element i in the mineral.

Experimental procedure

At room temperature, 1 g of chrysotile and 1 g of lizardite were each placed in separate 150 mL conical flasks (there were nine flasks for chrystotile and nine for lizardite, for each of the nine reaction times). Then, 100 mL of a 1.0 mol L^{-1} sulfuric acid solution was added to each flask, at a solid-to-liquid ratio of 1:100. The reaction times were 1, 2, 4, 12, 24, 72, 120, 168, or 216 h. In each case, the conical flask was placed in a shaker at a constant temperature, and the reaction was allowed to proceed fully. The reacted suspension was filtered to obtain the solid product and washed three times with distilled water until the pH of the filtrate was neutral. The solid product was dried in an oven at 60°C and set aside in a desiccator. The filtrate was collected in a 50 mL volumetric flask and left for subsequent testing. The sample labels were KS-T, where K is the mineral sample number, i.e., chrysotile is XS and lizardite is LS, S is the sulfuric acid medium, and T is the reaction time. To explore the commonalities and differences in the dissolution processes of chrysotile and lizardite, XRD, FTIR, inductively coupled plasma mass spectrometry (ICP-MS), and other analytical techniques were used. The mineral–water interface reaction rates of chrysotile and lizardite in sulfuric acid solution were compared by calculating the dissolution concentrations and dissolution rates of Si, Mg, and Fe in chrysotile and lizardite.

Results and Discussion

The results of X-ray fluorescence (XRF) spectroscopy analysis of the purified samples of chrysotile (XS) and lizardite (LS) are shown in Table 1. The main components of chrysotile are: w(SiO_2) = 41.69%, w(MgO) = 40.68% and w(Fe_2O_3) = 1.72% (where w(SiO_2 means the mass fraction of SiO_2 etc.). The main constituents of lizardite are: w(SiO_2) = 38.93%, w(MgO) = 37.46% and w(Fe_2O_3) = 6.88%. The crystal chemical formulae were calculated for serpentine using the (O) 14 oxygen atom calculation. Herein, the CaO and K_2O components were considered as impurities and were not involved in the crystal chemical formula calculation. The occupancy of each cation in the crystal structure was assigned according to the characteristics of the crystal structure of serpentine and the nature of the cations. In particular, Si^{4+}, Al^{3+} and Fe^{3+} occupy the tetrahedral position, and Mg^{2+}, Cr^{3+}, Ni^{2+} and Ti^{4+} occupy the octahedral positions (Caruso and Chernosky, 1979; Mellini and Zanazzi, 1987; Viti and Mellini, 1997; Fuchs et al., 1998). It was assumed that the ion positions and tetrahedral and octahedral sheets in chlorite and lizardite were the same; this would not affect the chemical formula of lizardite. Cations present in amounts of <0.001 atom in the composition were not included in the crystal formula. The crystal formulae calculated from the chemical analysis data are:

Chrysotile: $(Mg_{5.637}Fe_{0.031}Ni_{0.026}Ti_{0.007})[Si_{3.875}Al_{0.036}Fe_{0.089}O_{10}](OH)_8$; and
Lizardite: $(Mg_{5.302}Fe_{0.309}Cr_{0.027}Ni_{0.02}Ti_{0.007})[Si_{3.696}Al_{0.121}Fe_{0.183}O_{10}](OH)_8$.

Process of dissolution of Si, Mg, and Fe from chrysotile and lizardite in sulfuric acid solutions

Mineral–water interfacial reactions are related to the formation and transfer of charges which occur when substances on the mineral surface break bonds with the lattice, forming ions in the solution (Knauss and Wolery, 1988). Table 2 shows the ion dissolution content in the water interface reaction process of chrysotile and lizardite, and the ion dissolution concentration and dissolution rate are obtained by calculation. In sulfuric acid, the concentrations of Mg and Fe, from the chrysotile and lizardite sample solution, consistently exhibited an increasing trend as the reaction time

https://doi.org/10.1017/cmn.2024.26 Published online by Cambridge University Press

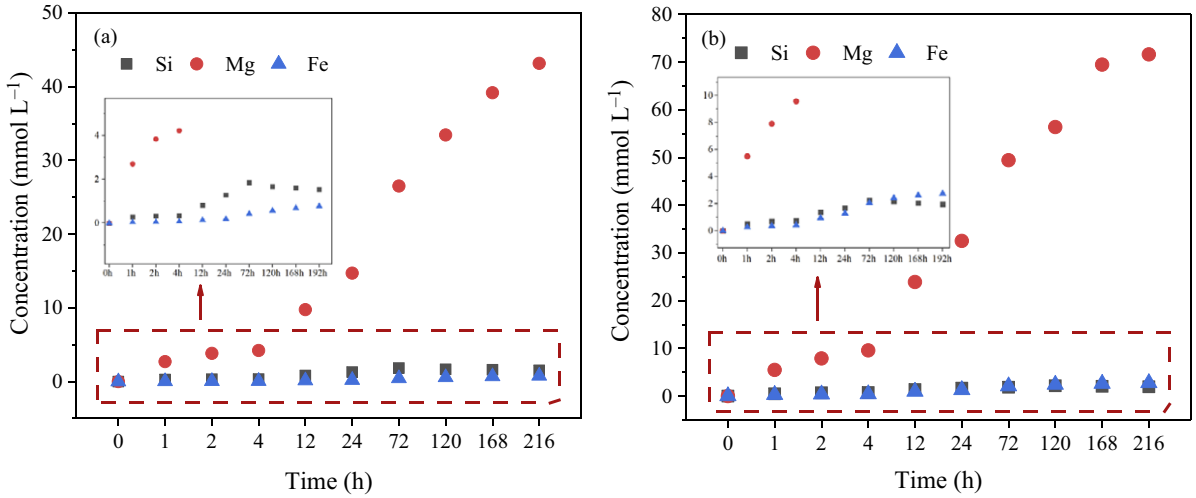

Figure 2. Variation in the dissolved concentration of ions in serpentine in sulfuric acid after various reaction times: (a) chrysotile; (b) lizardite.

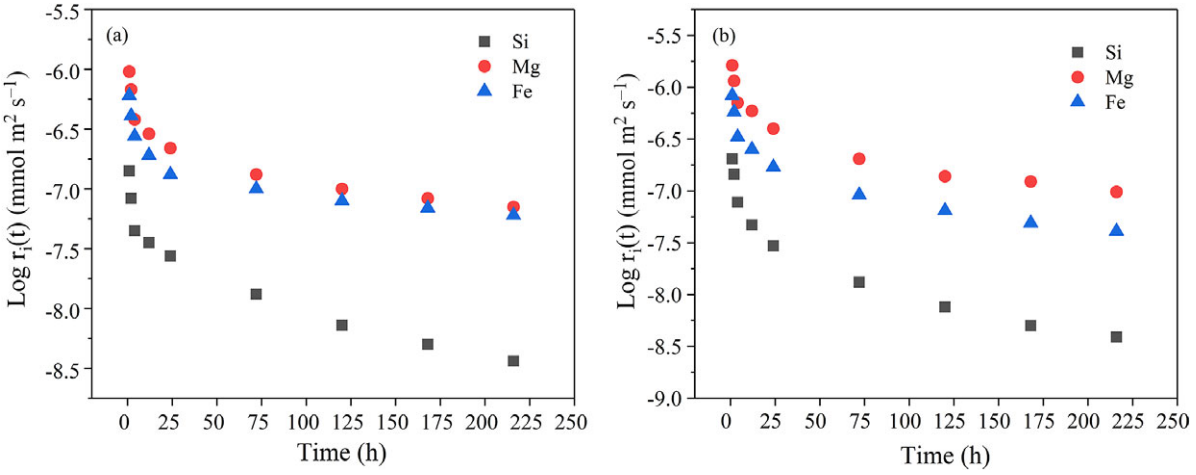

Figure 3. Variation in the rate of dissolution of ions from serpentine in sulfuric acid after different reaction times: (a) chrysotile; (b) lizardite.

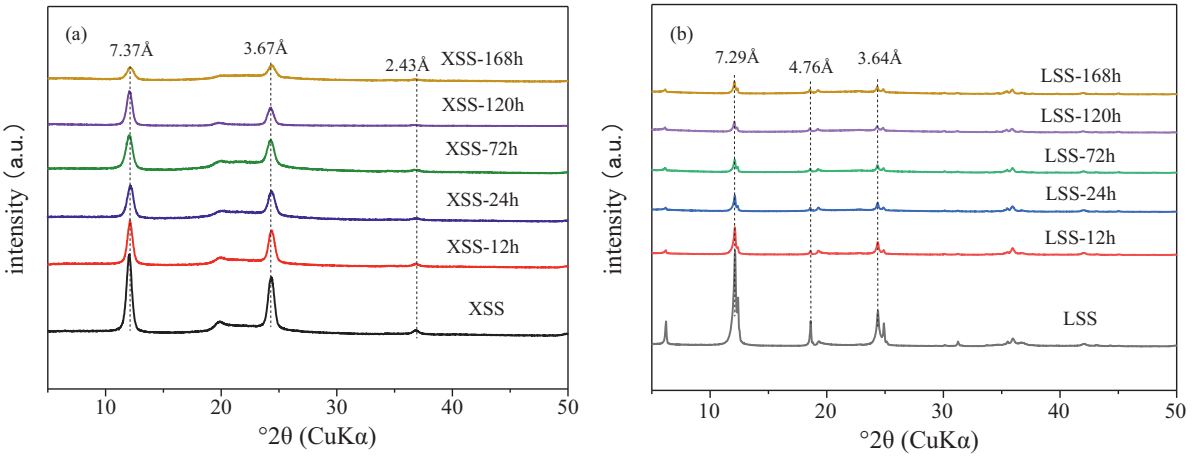

Figure 4. XRD results of serpentine products after various reaction times in sulfuric acid: (a) chrysotile; (b) lizardite.

increased (Fig. 2). When chrysotile was reacted in sulfuric acid for 216 h, the dissolved concentration of Mg was 43.16 mmol L^{-1}, and the dissolved concentration of Fe was 0.78 mmol L^{-1}. Additionally, when lizardite was reacted for 216 h, the dissolved concentration of Mg was 71.63 mmol L^{-1}, accompanied by a dissolved concentration of 2.74 mmol L^{-1} for Fe. Interestingly, the dissolved concentration of Si peaked at 72 and 120 h for chrysotile and lizardite, respectively. Dissolved Si then decreases due to the partial adsorption of Si by the

https://doi.org/10.1017/cmn.2024.26 Published online by Cambridge University Press

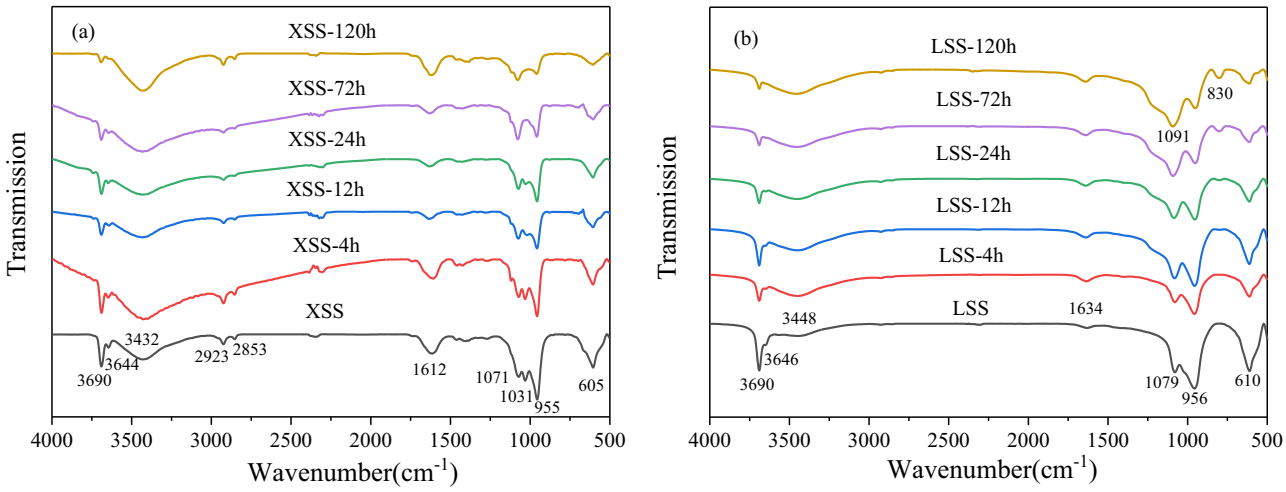

Figure 5. FTIR results of serpentine products after various reaction times in sulfuric acid: (a) chrysotile; (b) lizardite.

pores of the amorphous SiO_2 and the attachment of Si to the surface of the crystal structure for renucleation. Chrysotile and lizardite first exhibited the dissolution of Mg from the octahedral sheets in the mineral–water interfacial reaction. Si in the tetrahedral sheets then dissolved (Thom et al., 2013), followed by Fe. For lizardite the concentration of dissolved Fe exceeded that of Si at the late stage of the mineral–water interfacial reaction, and the dissolution concentration of each ion was greaterf than that of the chrysotile for the same reaction times. Regarding the ion dissolution concentrations, Mg leached easily from the mineral crystals in acidic media, and the dissolution concentration was greatest. The greater bond energy of Si–O compared with Mg–O led to easier bond breakage of the latter, and the complexation of Mg with the sulfuric acid solution, which promoted further dissolution of the octahedral sheets (Rozalen and Huertas, 2013).

In mineralogy, the macroscopic ion dissolution rate is usually related to the normalized reaction surface area. Based on the mineral, different models for normalizing the reaction surface area have been proposed: (1) the reaction surface area is usually assumed to be either the Brunauer–Emmett–Teller (BET) surface area of the mineral or proportional to the BET surface area (Ganor et al., 1999), and (2) the reaction surface area is confined to certain crystalline surfaces or is mainly controlled by surface defects. This work uses the BET surface area as the mineral–water interfacial reaction surface area. The measured BET specific surface area was 13.8 $m^2\ g^{-1}$ for chrysotile and 17.8 $m^2\ g^{-1}$ for lizardite. Chrysotile and lizardite react at the mineral–water interface in sulfuric acid, and the average dissolution rate of each ion continues to decrease as the reaction time increases, accompanied by an average dissolution rate: Mg>Fe>Si (Fig. 3). During the first 72 h of the reaction, the ions dissolved rapidly, and the mineral–water interface reaction took place vigorously. Over 72–216 h, the ion dissolution rate leveled off. In the presence of sulfuric acid, the dissolution concentrations of Mg, Si, and Fe and the average dissolution rates of lizardite were larger than those of chrysotile.

Structural changes of chrysotile and lizardite during reaction in sulfuric acid solutions

The XRD results for chrysotile demonstrate three diffraction peaks at d_{002} = 7.37 Å, d_{004} = 3.67 Å, and d_{202} = 2.45 Å (Fig. 4a). Lizardite is the main phase in the original sample, showing diffraction peaks at d_{001} = 7.29 Å, d_{110} = 4.76 Å, and d_{002} = 3.64 Å (Fig. 4b). A small amount of chlorite was detected, with diffraction peaks at d_{001} = 14.1 Å and d_{004} = 3.67 Å. On the one hand, the intensities of the characteristic peaks of both chrysotile and lizardite decrease with increasing mineral–water interfacial reaction time in sulfuric acid. This means that the octahedral sheets of both minerals are destroyed and Mg is gradually dissolved. On the other hand, the diffraction peak intensity of lizardite decreases more rapidly than that of chrysotile, suggesting that lizardite undergoes structural changes earlier during the reaction.

The FTIR results demonstrate that the intensity of the characteristic peaks of chrysotile (1071, 1031, and 955 cm^{-1}) and lizardite (1079 and 956 cm^{-1}) decreases with reaction time (Fig. 5). This indicates a disruption of the mineral structure and a gradual change to an amorphous SiO_2 structure (Farmer, 1974), leading to amorphization, which is related to the emergence of a new peak of lizardite at 830 cm^{-1}. The shift of the band at 1079 cm^{-1} to 1091 cm^{-1} (Fig. 5b) is associated with the vibrations of n(Si-O-Si) in amorphous silica (Rozalen and Huertas, 2013). The peak at 1031 cm^{-1} is attributed to the Si-O-Si vibration within the crystal perpendicular to the direction of the structure layer. The gradual disappearance of the peak strength proves that the environment of Si has changed substantially after the mineral–water interface reaction (Pentrák et al., 2010). Moreover, the increase of the band intensity at 3432 cm^{-1} (chrysotile) and 3448 cm^{-1} (lizardite) confirms that the siliceous by-product is hydrated (Rozalen and Huertas, 2013; Lacinska et al., 2016; Beglaryan et al., 2023). The intensity of the external Mg–OH bond (3690 cm^{-1}) stretching vibration decreases more rapidly than that of the internal Mg–OH bond (3644 and 3646 cm^{-1}) following the mineral–water interfacial reaction between the chrysotile and lizardite and the sulfuric acid solution, suggesting that the exposed external Mg is more susceptible to dissolution in acidic media (Liu et al., 2022). Moreover, the internal Mg-OH in chrysotile was still present at 120 h, while that of lizardite disappeared at 72 h. This indicates that the mineral–water interfacial reaction rate of lizardite is faster than that of chrysotile under the same conditions, which corresponds to the XRD data. The gradual disappearance of the characteristic peaks at 605 cm^{-1} for fibrous chrysotile and at 610 cm^{-1} for lizardite also confirms the gradual dissolution of Mg from the structure (Rozalen and Huertas, 2013).

The ^{29}Si MAS NMR results show that the main peaks of the Si spectra of chrysotile and lizardite are located at –95.88 and –93.99 ppm, respectively, attributed to the serpentine Q^3 type signal (Fig. 6)

https://doi.org/10.1017/cmn.2024.26 Published online by Cambridge University Press

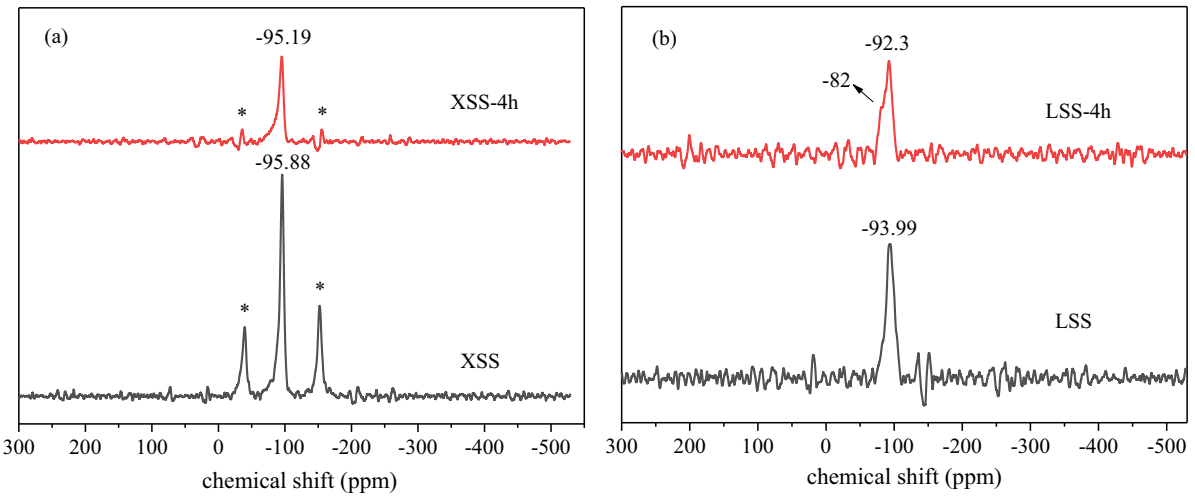

Figure 6. ^{29}Si MAS NMR results of serpentine products after 4 h of reaction in sulfuric acid: (a) chrysotile; (b) lizardite.

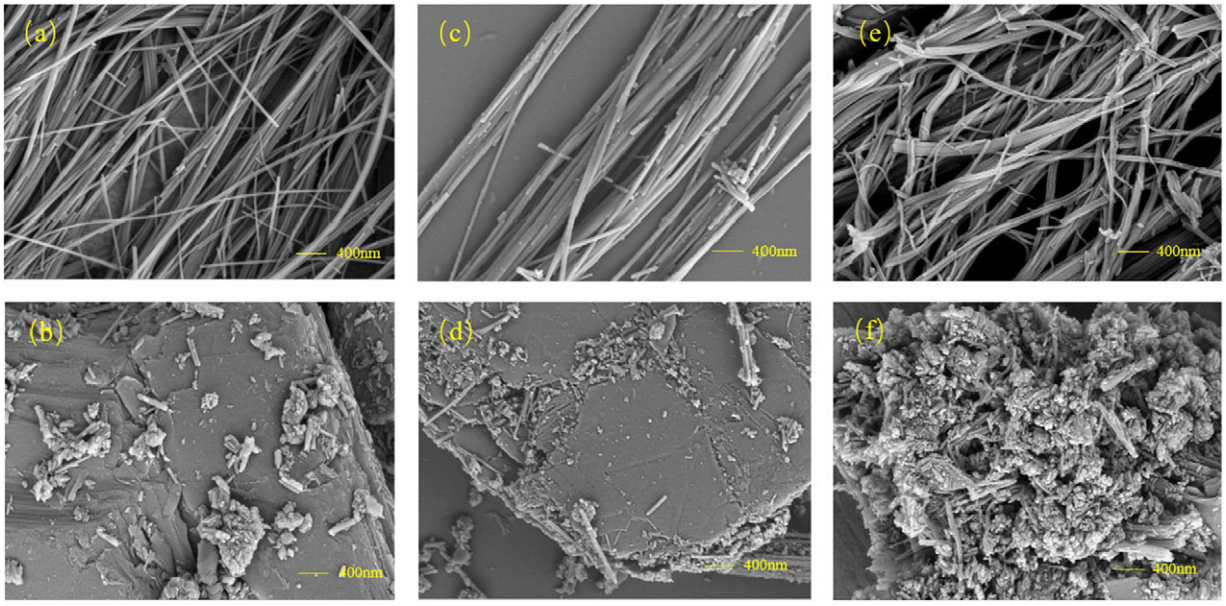

Figure 7. SEM images of serpentine products after different reaction times in sulfuric acid: (a) chrysotile; (b) lizardite; (c) chrysotile reacted for 24 h; (d) lizardite reacted for 24 h; (e) chrysotile reacted for 120 h; and (f) lizardite reacted for 120 h.

(Balucan, 2012). After 4 h of reaction time in the sulfuric acid medium for both minerals, the intensity of the main peak of chrysotile decreased (Fig. 6a), and no new peaks appeared. Lizardite showed a decrease in the intensity of the main peak (Fig. 6b), and a new peak at –82 ppm, which belongs to the chemical shift of ^{29}Si Q^2 (Magi et al., 1984). This implies that lizardite, compared with chrysotile, undergoes a chemical shift from the Q^3 structure to the Q^2 structures before the chemical change under sulfuric acid. This is consistent with the experimental results from ICP and XRD. Lizardite is more aggressively attacked by H^+, preferentially undergoing structural changes. Lizardite undergoes a chemical shift from the Q^3 to the Q^2 structure, probably due to the dissolution of Si leading to the breakage of the bridging oxygen bonds linking SiO_2 in the tetrahedra. Thus, lizardite is more aggressively attacked by H^+, preferentially undergoing structural changes.

Micromorphological changes of chrysotile and lizardite during reaction in sulfuric acid solutions

SEM results show that chrysotile (Fig. 7a) has an obvious tubular structure with a smooth surface. Lizardite has a complete lamellar structure with some small mineral particles attached to the surface (Fig. 7b). When chrysotile reacts with sulfuric acid at the mineral–water interface for 24 h, the surface smoothens and the tubular structure gradually disappears and becomes adherent to itself (Fig. 7c). After 24 h of the reaction of lizardite with sulfuric acid, the mineral is corroded by H^+, destroying part of the surface edge lamellar structure (Fig. 7d). Thus, the process of structural destruction of lizardite in acidic media proceeds from the surface to the interior. However, the destruction occurs preferentially at locations where the structure is weak or has excess surface energy and does not occur uniformly on all exposed surfaces. After 120 h of

https://doi.org/10.1017/cmn.2024.26 Published online by Cambridge University Press

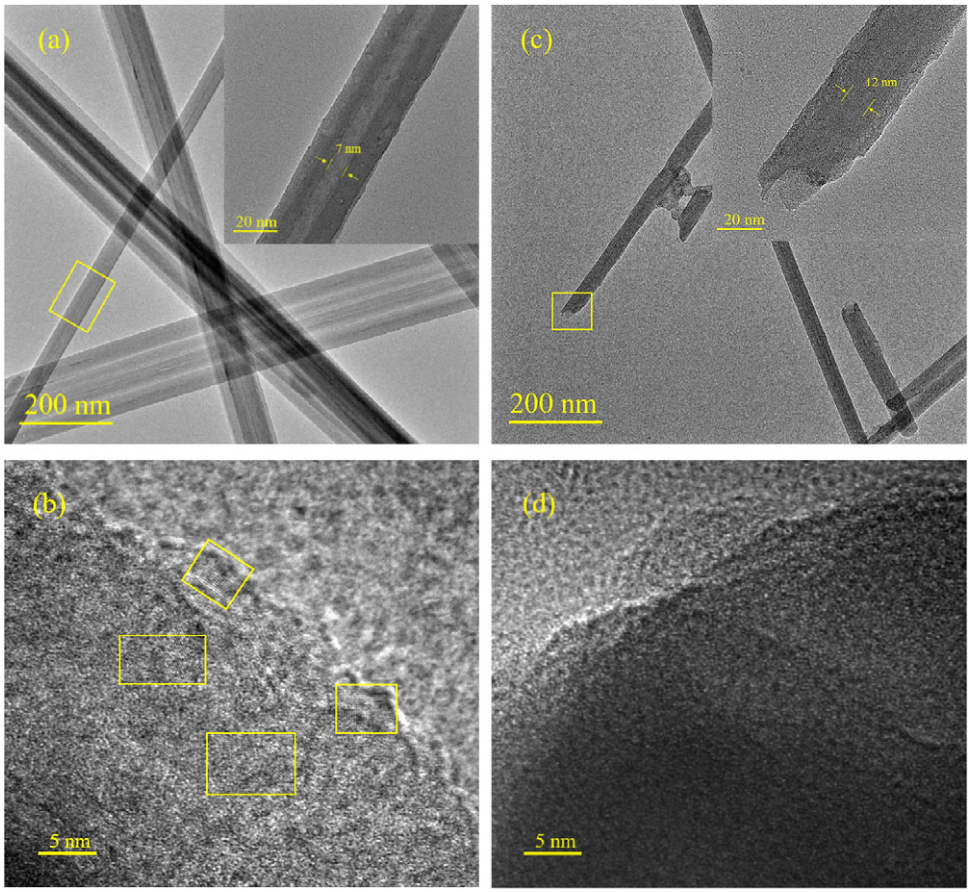

Figure 8. TEM images of serpentine products after 4 h of reaction in sulfuric acid: (a) chrysotile; (b) lizardite; (c) chrysotile reacted for 4 h; and (d) lizardite reacted for 4 h.

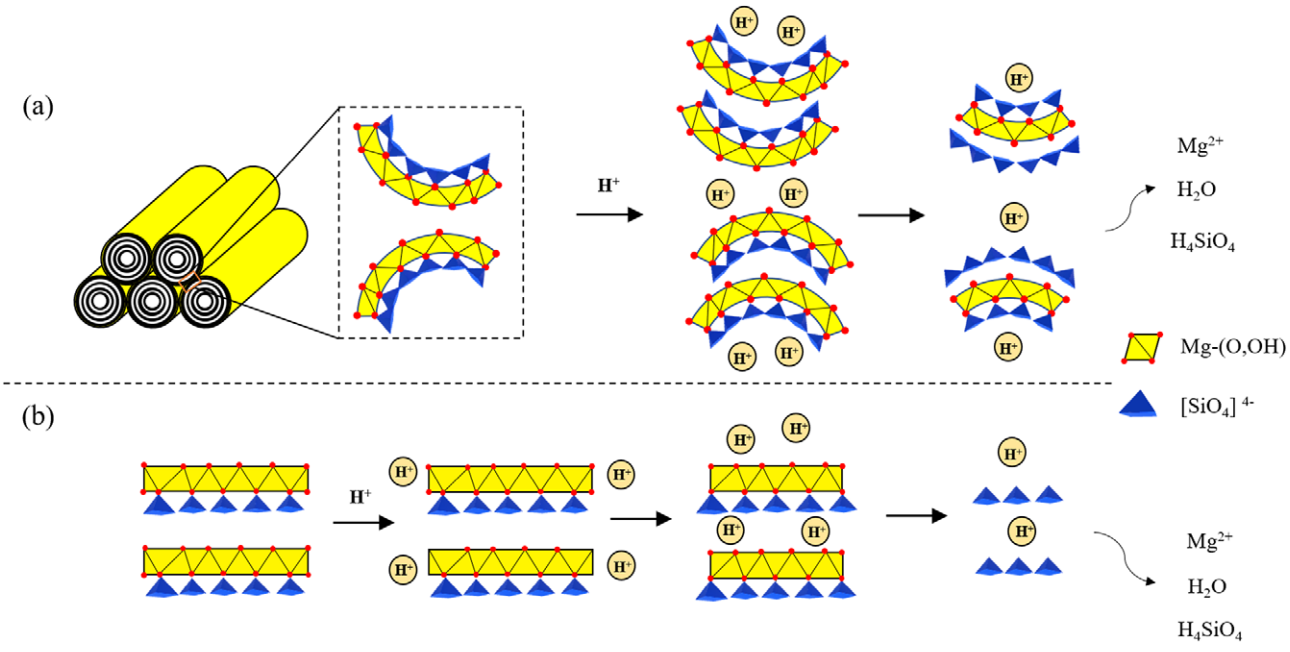

Figure 9. Schematic diagram of the serpentine structure attacked by H^+: (a) chrysotile; (b) lizardite.

reaction between the two minerals in the sulfuric acid solution (He et al., 2019), the edges, ends, and outer surfaces of the chrysotile were corroded (Fig. 7e). The corrosion can be attributed to the fracture of the external octahedral sheet M- (O, OH), resulting in bending and fracture. However, the fibrous tubular morphological features of chrysotile can still be seen. In contrast, lizardite was only partially laminated after 120 h of reaction, with most of the lamellar structure destroyed into amorphous SiO_2 aggregates (Fig. 7f).

https://doi.org/10.1017/cmn.2024.26 Published online by Cambridge University Press

Chrysotile has a single inner diameter of 7 nm and is structurally intact (Fig. 8a). The mineral–water interfacial reaction between chrysotile and sulfuric acid leads to the corrosion and dissolution of the edges of the fibrous tubes and the breakage and fragmentation of the long fibrous tubes, resulting in the formation of short tubes (Fig. 8c). Additionally, the inner wall of the fiber tube is also damaged by H^+ attack, leading to an increase in the inner diameter from 7 to 12 nm. Lizardite can clearly be seen as several lattice streaks in different directions, indicating a good crystallinity of lizardite (Fig. 8b). The lattice streaks become faint, indicating a decrease in lizardite crystallinity following a mineral–water interfacial reaction with sulfuric acid (Fig. 8d).

In summary, the mechanism of water interface reaction of chrysotile and lizardite in sulfuric acid medium is analyzed. The mineral–water interfacial reaction of lizardite in acidic media is stronger and faster than that of chrysotile. This can be attributed to the different structure of lizardite compared with chrysotile. Chrysotile has a tubular structure where the hydroxyl group in the outer octahedral sheet reacts with H^+ and the subsequent reaction is blocked by the inner silica-oxygen tetrahedral sheet blocking the subsequent reaction. The greater bond energy of Si–O compared with Mg- (O, OH) led to the dissolution rate of the silica-oxygen tetrahedral sheet being slower than that of the magnesium-oxygen octahedral sheet in acidic media. It is more stable, resulting in a weaker and less rapid reaction (Fig. 9a). Lizardite has a flat layer structure with small particles. After H^+ from the acidic medium enters the interlayer domain, it can react with the $(OH)^-$ group on each octahedral sheet, and the Mg in the mineral structure can dissolve quickly. The dissolution of Mg is not affected by the mineral structure. This results in the difference of dissolution between chrysotile and lizardite. The Si–O bond in the tetrahedral sheet is stronger than the Mg–(O, OH) bonds in the octahedral sheet. Therefore, Mg is dissolved preferentially (Fig. 9b).

Conclusions

In this work, the mineral–water interfacial reaction process between chrysotile and lizardite in acidic media was compared by XRD, FTIR, BET, SEM, TEM, and ^{29}Si MAS NMR techniques and by solution ICP-MS analysis. The conclusions are summarized as follows:

(1) For the mineral–water interfacial reaction process in the sulfuric acid medium, H^+ is more aggressive toward lizardite than chrysotile. As a result, the evolution of the lizardite structure is faster, and the ion dissolution rates and dissolution concentrations are greater than those of chrysotile. This is related to the different stacking structures of tetrahedral and octahedral sheets in lizardite and chrysotile. In addition, chrysotile and lizardite exhibited anisotropic dissolution in aqueous reactions in acidic media.

(2) The reaction of chrysotile and lizardite in an acidic medium also follows the same dissolution trend. In sulfuric acid solutions, Mg in the octahedral sheet dissolves first, while Si and Fe in the tetrahedral sheets dissolve later. Chrysotile and lizardite both show ion dissolution rates of Mg > Fe > Si.

(3) During the mineral–water interfacial reaction, the characteristic peaks of XRD and FTIR of chrysotile and lizardite weaken gradually, decreasing their peak intensities. The Si, Mg, and Fe components dissolve gradually and cause a gradual change in the chrysotile and lizardite structures.

In summary, the reactions of the two structurally different serpentines in acidic media have certain similarities and differences. This comparative study reveals the regularity of mineral–water interfacial reactions with composition and structural evolution for different layered serpentine types.

Author contribution. D.R. Zhao: Writing – original draft, Visualization, Software, Data curation. H.J. Sun and P.T. Jiang: Writing – review & editing, Validation, Supervision, Resources, Funding acquisition, Conceptualization. L. Zeng: Software, Methodology, Investigation.

Acknowledgements. None

Financial support. This study was supported by the National Natural Science Foundation of China (42072048).

Competing interest. The authors declare that they have no known competing financial interests or personal relationships that could have appeared to influence the work reported in this paper.

Data availability statement. Data will be made available on request.

References

Abad, I., Nieto, F., Reolid M., & Jiménez-Millán, J. (2022). Evidence of phyllosilicate alteration processes and clay mineral neoformation promoted by hydrothermal fluids in the Padul Fault area (Betic Cordillera, SE Spain). *Applied Clay Science*, *230*, 106669. https://doi.org/10.1016/j.clay.2022.106669.

Bailey, S. W. (1969). Polytypism of trioctahedral 1:1 layer silicates. *Clays and Clay Minerals*, *17*, 355–371. https://doi.org/10.1346/CCMN.1969.0170605

Balucan, R. D. (2012). Thermal studies of magnesium silicates from the great serpentinite belt in New South Wales for CO_2 sequestration by mineral carbonation in Australia. *The University of Newcastle Australia* 10.1021/acs.energyfuels.8b02823

Beglaryan, H., Isahakyan, A., Zulumyan, N., Melikyan, S., & Terzyan, A. (2023). A study of magnesium dissolution from serpentinites composed of different serpentine group minerals. *Minerals Engineering*, *201*, 108171. https://doi.org/10.1016/j.mineng.2023.108171

Bo, F., Lu, Y., Feng, Q., Peng, D., & Na, L. (2013). Mechanisms of surface charge development of serpentine mineral. *Transactions of Nonferrous Metals Society of China*, *23*, 1123–1128. https://doi.org/10.1016/S1003-6326(13)62574-1.

Caruso, L. J., & Chernosky, J. V. (1979). The stability of lizardite. *Canadian Mineralogist*, *17*, 757–769. WOS:000208514700010.

Corliss, J. B., Baross, J. A., & Hoffman, S. E. (1981). An hypothesis concerning the relationships between submarine hot springs and the origin of life on earth. *Oceanologica Acta, Special Issue*, SP, 59–69.

Daval, D., Hellmann, R., Martinez, I., Gangloff, S., & Guyot, F. (2013). Lizardite serpentine dissolution kinetics as a function of pH and temperature, including effects of elevated pCO_2. *Chemical Geology*, *351*, 245–256. https://doi.org/10.1016/j.chemgeo.2013.05.020

Evans, B.W. (2010). Lizardite versus antigorite serpentinite: magnetite, hydrogen, and life (?). *Geology*, *38*, 879–882. https://doi.org/10.1130/G31158.1

Farmer, V. C. (1974). The Layer Silicates. In: *The Infrared Spectra of Minerals*. The Mineralogical Society, London, pp. 331–363.

Farhang, F., Oliver, T. K., Rayson, M. S., Brent, G. F., Molloy, T. S., Stockenhuber, M., & Kennedy, E. M. (2019). Dissolution of heat activated serpentine for CO_2 sequestration: The effect of silica precipitation at different temperature and pH values. *Journal of CO_2 Utilization*, *30*, 123–129. https://doi.org/10.1016/j.jcou.2019.01.009

Fuchs, Y., Linares, J., & Mellini, M. (1998). Mössbauer and infrared spectrometry of lizardite-1T from Monte Fico, Elba. *Physics and Chemistry of Minerals*, *26*, 111–115. https://doi.org/10.1007/s002690050167

Ganor, J., Mogollón, J.L., & Lasaga, A.C. (1999). Kinetics of gibbsite dissolution under low ionic strength conditions. *Geochimica et Cosmochimica Acta*, *63*, 1635–1651. https://doi.org/10.1016/S0016-7037(99)00069-1

Habaue, S., Sato, K., Yamashita, K., Shimamura, T., Kaito, M., Masuda, T., & Kajiwara, M. (2008). Polysiloxanes derived from chrysotile asbestos via acid-leaching and silylation processes. *Journal of Applied Polymer Science*, *110*, 2891–2897. https://doi.org/10.1002/app.28899.

Hao, W., Flynn, S.L., Kashiwabara, T., Alam, M.S., Bandara, S., Swaren, L., & Konhauser, K.O. (2019). The impact of ionic strength on the proton reactivity of clay minerals. *Chemical Geology*, *529*, 119294. https://doi.org/10.1016/j.chemgeo.2019.119294.

He, H., Cao, J., & Duan, N. (2019). Defects and their behaviors in mineral dissolution under water environment: a review. *Science of the Total Environment*, *651*, 2208–2217. https://doi.org/10.1016/j.scitotenv.2018.10.151

Hermann, J. (2022). Cycles of serpentines. *Nature Geoscience*, *15*, 865–865.

Hirth, G., & Guillot, S. (2013). Rheology and tectonic significance of serpentinite. *Elements*, *9*, 107–113. https://doi.org/10.2113/gselements.9.2.107

Huang, R., Shang, X., Zhao, Y., Sun, W., & Liu, X. (2023). Effect of fluid salinity on reaction rate and molecular hydrogen (H_2) formation during Peridotite Serpentinization at 300°C. *Journal of Geophysical Research: Solid Earth*, *128*, e2022JB025218.

Knauss, K.G., & Wolery, T.J. (1988). The dissolution kinetics of quartz as a function of pH and time at 70°C. *Geochimica et Cosmochimica Acta*, *52*, 43–53. https://doi.org/10.1016/0016-7037(88)90055-5

Krevor, S.C., & Lackner, K.S. (2011). Enhancing serpentine dissolution kinetics for mineral carbon dioxide sequestration. *International Journal of Greenhouse Gas Control*, *5*, 1073–1080. https://doi.org/10.1016/j.ijggc.2011.01.006

Lacinska, A.M., Styles, M.T., Bateman, K., Wagner, D., Hall, M.R., Gowing, C., & Brown, P.D. (2016). Acid-dissolution of antigorite, chrysotile and lizardite for ex situ carbon capture and storage by mineralisation. *Chemical Geology*, *437*, 153–169. https://doi.org/10.1016/j.chemgeo.2016.05.015

Lavkulich, L.M., Schreier, H.E., & Wilson, J.E. (2014). Effects of natural acids on surface properties of asbestos minerals and kaolinite. *Journal of Environmental Science and Health, Part A*, *49*, 617–624. https://doi.org/10.1080/10934529.2014.865401

Li, Q., Li, J., & Zhu, B. (2022). Experimental investigation of the influence of sequential water-rock reactions on the mineral alterations and porosity evolution of shale. *Construction and Building Materials*, *317*, 125859. https://doi.org/10.1016/j.conbuildmat.2021.125859

Liu, W., Peng, X., Liu, W., Zhang, N., & Wang, X. (2022). A cost-effective approach to recycle serpentine tailings: destruction of stable layered structure and solvent displacement crystallization. *International Journal of Mining Science and Technology*, *32*, 595–603. https://doi.org/10.1016/j.ijmst.2022.03.004

Liu, K., Feng, Q., Yang, Y., Zhang, G., Ou, L., & Lu, Y. (2007). Preparation and characterization of amorphous silica nanowires from natural chrysotile. *Journal of Non-Crystalline Solids*, *35*, 1534–1539. https://doi.org/10.1016/j.jnoncrysol.2007.01.033

Liu, X., Ma, Y., Yan, W., He, M., Li, L., Sui, X., & Peng, B. (2023). Identify key serpentines antigorite, lizardite and chrysotile with various compositions and crystallographic orientations using micro-Raman spectroscopy. *Solid Earth Sciences*, *8*, 295–304. https://doi.org/10.1016/j.sesci.2023.10.003

Locati, F., Collo, G., Madsen, L., Muñoz, M., Marfil, S., & Maiza, P. (2022). Clay mineral assemblages as the key to understanding alteration processes in basalts from the province of Corrientes, Argentina. *Journal of South American Earth Sciences*, *116*, 103777. https://doi.org/10.1016/j.jsames.2022.103777

Magi, M., Lippmaa, E., Samoson, A., Engelhardt, G., & Grimmer, A.R. (1984). Solid-state high-resolution silicon-29 chemical shifts in silicates. *Journal of Physical Chemistry*, *88*, 1518–1522. https://doi.org/10.1021/j150652a015

Mével, C. (2003). Serpentinization of abyssal peridotites at mid-ocean ridges. *Comptes Rendus Geoscience*, *335*, 825–852. https://doi.org/10.1016/j.crte.2003.08.006

Mellini, M., & Zanazzi, P.F. (1987). Crystal structures of lizardite-1T and lizardite-2H1 from Coli, Italy. *American Mineralogist*, *72*, 943–948.

Palmieri, F., Estoppey, A., House, G.L., Lohberger, A., Bindschedler, S., Chain, P. S., & Junier, P. (2019). Oxalic acid, a molecule at the crossroads of bacterial-fungal interactions. *Advances in Applied Microbiology*, *106*, 49–77. https://doi.org/10.1016/bs.aambs.2018.10.001

Pentrák, M., Madejová, J., & Komadel, P. (2010). Effect of chemical composition and swelling on acid dissolution of 2:1 clay minerals. *Philosophical Magazine*, *90*, 2387–2397. https://doi.org/10.1080/14786430903559433

Ren, Y., Cao, X., Wu, P., & Li, L. (2023). Experimental insights into the formation of secondary minerals in acid mine drainage-polluted karst rivers and their effects on element migration. *Science of the Total Environment*, *858*, 160076. https://doi.org/10.1016/j.scitotenv.2022.160076

Rozalen, M., & Huertas, F.J. (2013). Comparative effect of chrysotile leaching in nitric, sulfuric and oxalic acids at room temperature. *Chemical Geology*, *352*, 134–142. https://doi.org/10.1016/j.chemgeo.2013.06.004

Sanna, A., Wang, X., Lacinska, A., Styles, M., Paulson, T., & Maroto-Valer, M.M. (2013). Enhancing Mg extraction from lizardite-rich serpentine for CO_2 mineral sequestration. *Minerals Engineering*, *49*, 135–144. https://doi.org/10.1016/j.mineng.2013.05.018

Silva, S.P., Wander, A.P., Bisatto, R., & Galland, G.B. (2011). Preparation and characterization of chrysotile for use as nanofiller in polyolefins. *Nanotechnology*, *22*, 105701.

Sleep, N.H., Meibom, A., Fridriksson, T., Coleman, R.G., & Bird, D.K. (2004). H_2-rich fluids from serpentinization: geochemical and biotic implications. *Proceedings of the National Academy of Sciences*, *101*, 12818–12823. https://doi.org/10.1073/pnas.0405289101

Thom, J.G., Dipple, G.M., Power, I.M., & Harrison, A.L. (2013). Chrysotile dissolution rates: implications for carbon sequestration. *Applied Geochemistry*, *35*, 244–254. https://doi.org/10.1016/j.apgeochem.2013.04.016.

Thomassin, J.H., Goni, J., Baillif, P., Touray, J.C., & Jaurand, M.C. (1977). An XPS study of the dissolution kinetics of chrysotile in 0.1 N oxalic acid at different temperatures. *Physics and Chemistry of Minerals*, *1*, 385–398. https://doi.org/10.1007/BF00308848

Turci, F., Tomatis, M., Mantegna, S., Cravotto, G., & Fubini, B. (2007). The combination of oxalic acid with power ultrasound fully degrades chrysotile asbestos fibres. *Journal of Environmental Monitoring*, *9*, 1064–1066. https://doi.org/10.1039/B709571F

Turci, F., Tomatis, M., Mantegna, S., Cravotto, G., & Fubini, B. (2008). A new approach to the decontamination of asbestos-polluted waters by treatment with oxalic acid under power ultrasound. *Ultrasonics Sonochemistry*, *15*, 420–427. https://doi.org/10.1016/j.ultsonch.2007.08.007

Valouma, A., Verganelaki, A., Maravelaki-Kalaitzaki, P., & Gidarakos, E. (2016). Chrysotile asbestos detoxification with a combined treatment of oxalic acid and silicates producing amorphous silica and biomaterial. *Journal of Hazardous Materials*, *305*, 164–170. https://doi.org/10.1016/j.jhazmat.2015.11.036.

Viti, C., & Mellini, M. (1997). Contrasting chemical compositions in associated lizardite and chrysotile in veins from Elba, Italy. *European Journal of Mineralogy-Ohne Beihefte*, *9*, 585–596.

Wang, L., Lu, A., Wang, C., Zheng, X., Zhao, D., & Liu, R. (2006). Nano-fibriform production of silica from natural chrysotile. *Journal of Colloid and Interface Science*, *295*, 436–439. https://doi.org/10.1016/j.jcis.2005.08.055

https://doi.org/10.1017/cmn.2024.26 Published online by Cambridge University Press